Sphingomyelin metabolism is involved in the differentiation of MDCK cells induced by environmental hypertonicity

Nicolás Octavio Favale,*,† Bruno Jaime Santacreu,*,† Lucila Gisele Pescio,*,† Maria Gabriela Marquez,†,§ and Norma Beatriz Sterin-Speziale[1,†]

Facultad de Farmacia y Bioquímica,* Universidad de Buenos Aires, Argentina; IQUIFIB-LANAIS-PROEM-CONICET,† Ciudad Autónoma de Buenos Aires, Argentina; and Instituto de Investigaciones en Ciencias de la Salud Humana (IICSHUM),§ Universidad Nacional de La Rioja , La Rioja, Argentina

Abstract Sphingolipids (SLs) are relevant lipid components of eukaryotic cells. Besides regulating various cellular processes, SLs provide the structural framework for plasma membrane organization. Particularly, SM is associated with detergent-resistant microdomains. We have previously shown that the adherens junction (AJ) complex, the relevant cell-cell adhesion structure involved in cell differentiation and tissue organization, is located in an SM-rich membrane lipid domain. We have also demonstrated that under hypertonic conditions, Madin-Darby canine kidney (MDCK) cells acquire a differentiated phenotype with changes in SL metabolism. For these reasons, we decided to evaluate whether SM metabolism is involved in the acquisition of the differentiated phenotype of MDCK cells. We found that SM synthesis mediated by SM synthase 1 is involved in hypertonicity-induced formation of mature AJs, necessary for correct epithelial cell differentiation. Inhibition of SM synthesis impaired the acquisition of mature AJs, evoking a disintegration-like process reflected by the dissipation of E-cadherin and β- and α-catenins from the AJ complex. As a consequence, MDCK cells did not develop the hypertonicity-induced differentiated epithelial cell phenotype.—Favale, N. O., B. J. Santacreu, L. G. Pescio, M. G. Marquez, and N. B. Sterin-Speziale. **Sphingomyelin metabolism is involved in the differentiation of MDCK cells induced by environmental hypertonicity. *J. Lipid Res.* 2015.** 56: **786–800.**

Supplementary key words sphingomyelin synthase • renal epithelial cells • Madin-Darby canine kidney cells

Sphingolipids (SLs) are relevant components of the eukaryotic membrane. Besides providing a structural framework for plasma membrane (PM) organization, SLs regulate various cellular processes such as growth, death, differentiation, and intracellular trafficking (1). It has been demonstrated that cells adjust SL production in response to metabolic needs (2). SM is biochemically synthesized through the activity of serine-palmitoyl-CoA transferase, 3-ketosphinganine reductase, ceramide (Cer) synthase, dihydroceramide desaturase, and sphingomyelin synthase (SMS). SMS, which uses Cer and phosphatidylcholine as substrates, is the last enzyme in SM biosynthesis (3). Two isoforms, SMS1 and SMS2, have been cloned in mammals (4). SMS1 localizes in the Golgi apparatus, whereas SMS2 can be localized in the PM (5) but also in the Golgi apparatus. Although SM is principally synthesized by SMS1 activity, it has been reported that both SMS1 and SMS2 are required for SM homeostasis and growth in human HeLa cells (6). SM synthesis is directly related to correct intracellular protein trafficking (7). It has been recently shown that the downregulation of SMSs significantly retards the trafficking of the reporter protein vesicular stomatitis virus G protein tagged with GFP from the trans-Golgi network to the PM. Moreover, the correct endosomal recycling network is directly related to Golgi SM synthesis (8).

SM is the main SL in mammalian cells. Because of the high affinity of interaction with cholesterol, SM drives the formation of PM rafts or detergent-resistant microdomains (DRMs) (9, 10), thus providing a framework for PM organization. Early studies have demonstrated

This work was supported by grants from the University of Buenos Aires (UBACYT-20020100300066 and UBACYT-200201001006092), CONICET (PIP 112-200801-00233 and PIP 413), and ANPCyT (PICT 01038 and PICT 01625), Argentina. The authors have no disclosures relevant to this study.

Manuscript received 20 May 2014 and in revised form 27 January 2015.

Published, JLR Papers in Press, February 10, 2015
DOI 10.1194/jlr.M050781

Abbreviations: AJ, adherens junction; C_6-NBD-Cer, C6-NBD-ceramide; Cer, ceramide; D609, tricyclodecan-9-yl-xanthogenate; DIC, differential interference contrast; D-PDMP, D-threo-1-phenyl-2-decanoylamino-3-morpholino-1-propanol; GlcCer, glucosylceramide; HPTLC, high-performance TLC; LacCer, lactosylceramide; LDH, lactate dehydrogenase; MDCK, Madin-Darby canine kidney; Myr, myriocin; PM, plasma membrane; qRT-PCR, quantitative RT-PCR; SL, sphingolipid; SMS, sphingomyelin synthase; SPT, serine palmitoyl transferase.

[1]To whom correspondence should be addressed.
e-mail: speziale@ffyb.uba.ar

that rafts play important roles in signal transduction and protein sorting in cell membranes (11, 12). Rafts have been also associated with regulation of the actin cytoskeleton and the cell matrix and cell-cell adhesion structures (13–16). We have recently demonstrated that in fully differentiated collecting duct cells, adherens junction (AJ) protein complexes are located in an SM-cholesterol-rich DRM, whose lipid composition is necessary to preserve cell-cell adhesion (17).

Cultured Madin-Darby canine kidney (MDCK) cells are used as a model to study epithelial cell polarization and differentiation. When seeded at low density, MDCK cells undergo morphological changes from a fibroblast-like phenotype to a polarized one (18). To acquire a polarized phenotype, MDCK cells have to adhere to each other, and such adhesion is essential to the maintenance of tissue integrity. The first step in cell-cell adhesion is the establishment of AJ by homophilic cadherin interaction of adjacent cells and the intracellular formation of the AJ complex (19). The interaction of E-cadherin with neighboring cells recruits downstream β-catenin, p120-catenin, and α-catenin, which link and modulate the organization of the actin cytoskeleton (20) and form mature AJs. As a result, each component in the E-cadherin, β-catenin, α-catenin, and actin cytoskeleton complex is important in maintaining the stability of AJs (21). Initially, the AJ complex is immature and unstable, but as cells undergo differentiation, the AJ complex matures and becomes stable. In this process, the E-cadherin-mediated AJ complex is critical for the maintenance of the epithelial tissue architecture (22–24).

In our lab, we have demonstrated that under hypertonic conditions, MDCK cells acquire a differentiated phenotype with changes in the cellular and nuclear architecture (25, 26), accompanied by changes in lipid metabolism (27, 28). Considering both that AJ plays a central role in epithelial cell differentiation and our previous observation that AJ is located in an SM-rich membrane domain, we decided to evaluate whether SM synthesis is involved in the acquisition of the differentiated phenotype of MDCK cells induced by external hypertonic stress.

MATERIALS AND METHODS

Cell culture, treatment, and transfection

MDCK cells were seeded at a density of 0.1×10^6 cells/ml in 6-well multidishes and grown in DMEM (GIBCO) containing 10% FBS, penicillin (100 μg/ml), and streptomycin (100 μg/ml) at 37°C in a humidified 5% CO_2 atmosphere. After 24 h, the medium was replaced by DMEM containing 0.5% FBS so as to synchronize the cell cycle, and cells were incubated for another 24 h to reach confluence. In this condition, MDCK cells acquired a polarized phenotype. Then, cells were switched to a hypertonic medium (550 mOsm) by addition of NaCl and further incubated for 48 h. To inhibit SMS activity, tricyclodecan-9-yl-xanthogenate (D609; Sigma-Aldrich), an SMS inhibitor, was used at 7.5, 10, 15, and 20 μM. It is important to note that these D609 concentrations were adjusted to inhibit SMS activity and maintain cell viability (~100%). D609 was added to the culture medium, together with hypertonic treatment. Cells subjected to isotonic conditions were incubated for the same periods of time but in isotonic medium. To inhibit serine-palmitoyl-CoA transferase, myriocin (Myr; Sigma-Aldrich), a specific inhibitor, was used at 100 nM. To inhibit glucosylceramide (GlcCer) synthase activity, D-threo-1-phenyl-2-decanoylamino-3-morpholino-1-propanol (D-PDMP; Matreya), was used at 5 μM. Both inhibitors were added to the culture medium, together with hypertonicity and/or D609 treatment. To obtain SMS1 and SMS2 siRNA-transfected cells, 4 h before subjection to hypertonicity, confluent MDCK cells were seeded and transfected with 40 nM SMS1 siRNA duplex 5′-ACCUGUUGCACCGAUAUUCAATT-3′ 5′-UUGAAUAUCGGUGCAACAGGUTT-3′ (Gene ID: 477582, sphingomyelin synthase 1, *Canis lupus familiaris*) and with 40 nM SMS2 siRNA duplex 5′-GGCACCAAAAAGTACCCAGA-3′ 5′-GAGTCTCCGTTGAGCTTTGG-3′ (Gene ID: 478505, sphingomyelin synthase 2, *Canis lupus familiaris*) (Invitrogen) by using HiPerFect Transfection Reagent (QIAGEN), following the manufacturer's protocol. Efficacy was determined by cotransfection with siRNA conjugated with AlexaFluor 488 (AllStars Negative Controls-QUIAGEN). Positive intracellular green dots were considered as positive as transfected. The transfection efficacy was between 15% and 25%.

Lipid analysis

MDCK cells were treated as described above and labeled with 25 nCi/ml of [^{14}C]palmitic acid (PerkinElmer) or 2 μCi/ml of [^{14}C]serine (PerkinElmer). After 18 h of incubation, the cells were harvested and lipids extracted by the Bligh and Dyer technique and dried by N_2. Glycerophospholipids were removed by saponification in alkaline methanol, followed by reextraction and evaporation. Aliquots of SLs were spotted onto a TLC plate. The corresponding radioactive spots were scraped off the TLC plates for additional measurement by liquid scintillation counting. Data were normalized to the number of counts incorporated every 10^6 cells.

For SM analysis, the TLC was developed in chloroform-methanol-acetic acid-water (40:10:10:1, v/v/v/v) and visualized by autoradiography. For Cer, GlcCer, and lactosylceramide (LacCer) analysis, the TLC was developed in two different solvents. The first TLC was developed to two-thirds of the plate in solvent system butanol-acetic acid-water (60:20:20, v/v/v). Then, the plate was cut at Rf = 0.8 (just above the sphingosine standard), and the remaining piece of the plate was developed in choloform-methanol (98:2, v/v). The radioactive spots were visualized by autoradiography. Endogenous content of Cer was determined by densitometric analysis by using copper acetate reagent as described by Fewster et al. (29). Results are expressed as relative percentage of the control. Endogenous content of SM was carried out by measuring the quantity of free orthophosphate using Fiske-Subbarow reagent (30).

Before the radioactive incorporation experiments, the SLs were identified by mass spectroscopy analysis. The TLC was revealed by the primuline staining technique (31) and visualized under UV light. The bands corresponding to the Rf of the different standards were scraped off and separated from the plate by extraction. This was performed by three successive extractions with chloroform-methanol-water (5:5:1, v/v/v), thoroughly mixing, centrifuging, collecting the solvents, and partitioning with 4 vol of water to recover the lipids in the chloroform phase (32). This phase was evaporated under N_2 flow, and the samples were analyzed by MALDI TOF-TOF analysis at LANAIS-PROEM-CONICET, Argentina. The standards used were as follows: C12:0 SM (d18:1/12:0; *N*-lauroyl-D-erythro-sphingosylphosphorylcholine),

C12:0 Cer (d18:1/12:0; *N*-lauroyl-D-erythro-sphingosine), C12:0 GlcCer (d18:1/12:0; D-glucosyl-β-1,1' *N*-lauroyl-D-erythro-sphingosine), C18:0 GlcCer (d18:1/18:0; D-glucosyl-β-1,1' *N*-stearoyl-D-erythro-sphingosine), C12:0 LacCer (d18:1/16:0; D-lactosyl-β-1,1' *N*-laurosyl-D-erythro-sphingosine), and sphingosine (d18:1; D-erythro-sphingosine), all from Avanti Polar Lipids Inc.

Fluorescence microscopy

Cells were plated on coverslips and treated as described above. Cells were washed with PBS, fixed with 4% (w/v) paraformaldehyde at 25°C for 20 min, and permeabilized with 0.1% (v/v) Triton X-100 at 25°C for 20 min. After washing with PBS, cells were incubated with 3% BSA and 3% normal goat serum in PBS at 25°C for 60 min, followed by incubation at 25°C for 90 min with different primary antibodies. The antibodies used were as follows: 1:250 mouse anti-β-catenin (Sigma), 1:200 rabbit anti-α-catenin (Sigma), and 1:50 rabbit anti-E-cadherin (Santa Cruz Biotechnology). Primary interactions were detected by using a 1:100 $F(ab')^2$ fragment of goat anti-rabbit IgG and a 1:100 $F(ab')^2$ fragment of goat anti-mouse IgG (Jackson ImmunoResearch), both FITC- and tetramethylrhodamine-labeled. For actin filament observation, the marker phalloidin-FITC (Sigma) with primary antibodies was used.

The detection of PM level of SM was performed by lysenin (PeptaNova) staining as described by Yamaji et al. (33) and modified by Barceló-Coblijn et al. (34). Lysenin was detected by using a 1:200 rabbit anti-lysenin antibody (PeptaNova) and a 1:200 $F(ab')^2$ fragment of goat anti-rabbit IgG, Alexa Fluor 647 conjugated (Molecular Probes). The coverslips were then mounted onto microscope glass slides with Vectashield Mounting Medium (Vector Laboratories) and stored at 4°C until analysis.

A nonsilencing siRNA conjugated with AlexaFluor 488 (AllStars Negative Controls, QIAGEN) was used as a control and for monitoring transfection. Labeled cells were analyzed for the evaluation of morphological changes induced by specific siRNAs.

Imaging and data processing

Cells were examined by wide-field microscopy with an epifluorescence Nikon Eclipse Ti microscope equipped with an oil immersion 60× numerical aperture 1.40. Images were taken with the acquisition freeware Micrometric SE premium. A minimum of 10 fields containing several cells were collected from each sample. Images of confocal immunofluorescence were obtained by an Olympus FV300 confocal microscope (model BX61) equipped with Ar and He-Ne lasers, and oil immersion 60× numerical aperture 1.40. Images were taken with the acquisition software FluoView version 3.3. A minimum of 10 fields containing several cells were collected from each sample. Optical sections of 0.5 µm for z-plane and 3D reconstruction were obtained. Images were analyzed and reconstructed using ImageJ and Image-Pro plus version 4.5.

Immunoblotting

After washing with PBS, cells were treated with trypsin-EDTA and counted, and viability was determined by the trypan-blue exclusion assay. After resuspending in lysis buffer (50 mM HEPES, 1% Triton ×100, 150 mM NaCl, 1 mM PMSF, 1 µg/ml aprotinin, 1 mM leupeptin, 200 µM $NaVO_4$), cells were passed through a 29-gauge needle, and aliquots of either 20,000 or 30,000 cells were incubated with 4× Laemmli buffer at 100°C for 5 min and resolved in a 10% or 12.5% SDS-polyacrylamide gel and blotted to polyvinylidene fluoride membranes. In the E-cadherin experiments, cells were scraped off with a rubber policeman. Blots were blocked with 10% nonfat milk in TBS-Tween incubated overnight at 4°C with 1:5,000 mouse anti-α-catenin, 1:5,000 rabbit anti-β-catenin, and 1:500 rabbit anti-E-cadherin in 1% BSA in TBS-Tween. After washing, blots were incubated with secondary antibodies and bands evidenced by means of the Bio-Lumina analysis system (Kalium Technologies). The intensity of each band was estimated by optical densitometry using ImageJ software.

mRNA measurements

Total RNA was isolated with RV Total RNA isolation reagent (Promega). SMS1 and SMS2 mRNA levels were measured by semiquantitative RT-PCR (18–30 cycles) from 0.4 µg in total RNA. To compare the relative mRNA levels, both SMS1 and SMS2 were determined in the same reaction. The forward and reverse primer sequences were SMS1: 5′-CCGAAGCTTTTTGGAGACTG-3′ and 5′-ATGCAGAAGATCCCAACCAC-3′; SMS2: 5′-GGCACCAAAAAGTACCCAGA-3′and 5′-GAGTCTCCGTTGAGCTTTGG-3. A negative control was performed by omitting the cDNA sample. For real-time PCR [quantitative RT-PCR (qRT-PCR)], a new set of primers was designed: SMS1:5′-CCTGTCCATCACTGGTTCT-3′ and 5′-ATGCAGAAGATCCCAACCAC-3′; SMS2: 5′-ACGGAGACTCTCAGGCAAAA-3′ and 5′-TCAGCACAACAGTGTGACCA-3. Beta actin was used as control. The qRT-PCR was performed in a RotorGene Q (QIAGEN).

SMS enzyme assay

The SMS enzyme assay was adapted from the protocol developed by van Helvoort et al. (35) and modified by Ternes et al. (36). MDCK cells treated as described above were washed twice with HBSS and incubated with HBSS containing 1% w/v fatty acid-free BSA (HBGB) and 2 µM C_6-NBD-ceramide (C_6-NBD-Cer; Molecular Probe) at 4°C for 4 h. The incubation supernatant was saved, and cells were incubated again with HBGB (without C_6-NBD-Cer) at 4°C for 30 min. The new supernatant was saved and pooled with the first one. The cells were washed twice with HBSS and scraped off. Lipids were extracted from cells, and supernatants by the Bligh and Dyer technique. The lipid extract was analyzed by high-performance TLC (HPTLC) in chloroform-acetone-methanol-acetic acid-water (50:20:10:10:5, v/v/v/v/v). Fluorescent lipids were visualized on a STORM 860 Image Analysis system (Molecular Dynamics), and the relative intensity of the band was quantified using ImageJ software. To identify SM, GlcCer, and LacCer spots, standards for C12:0 SM, C18:0 GlcCer, and C12:0 LacCer were used (Avanti Polar Lipids Inc.). The presence of the standards was revealed by the primuline technique.

Lactate dehydrogenase assay

The lytic lysenin activity was assessed by the determination of the released lactate dehydrogenase (LDH) in the medium, measured by an LDH-P UV assay kit (Wiener Laboratorios, Rosario, Argentina) according to the manufacturer's instructions. The maximum amount of releasable LDH enzyme activity was determined by lysing the cells with 0.2% Tween 20.

RESULTS

SMS1 expression and activity are increased during induced MDCK differentiation

MDCK morphological changes were evaluated by differential interference contrast (DIC) microscopy. Confluent MDCK cells cultured in isotonic medium displayed an elongated fibroblast-like phenotype (**Fig. 1A**-a), whereas, when cultured in hypertonic medium

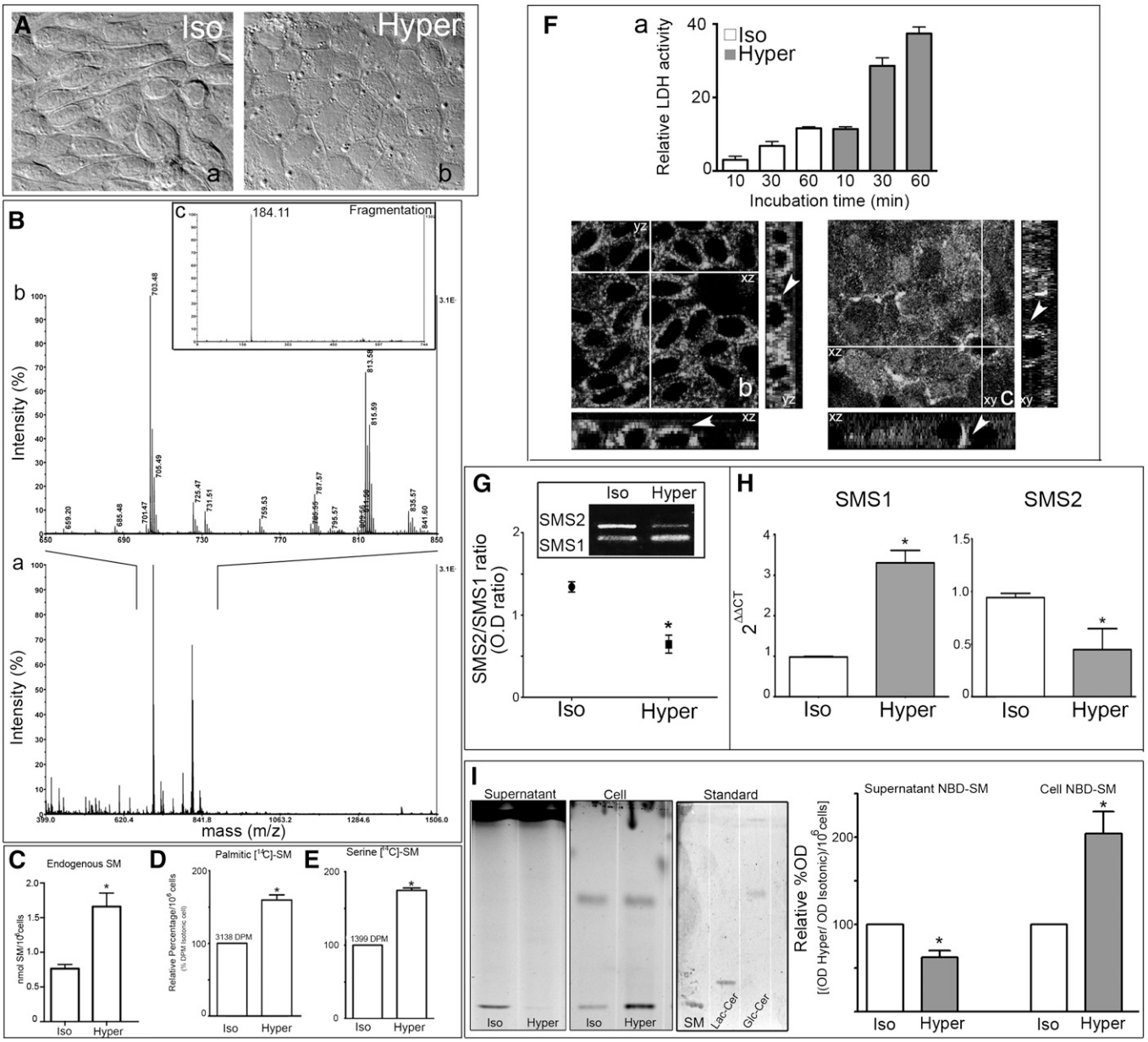

Fig. 1. SMS1 expression and activity are increased during induced MDCK differentiation. MDCK morphological changes were evaluated by DIC microscopy. A: Confluent MDCK cells cultured in isotonic medium (a) and subjected to external hypertonicity for 48 h (b). B: MALDI TOF/TOF analysis of the TLC spot corresponding to the Rf of SM. The intensity versus mass (*m/z*) graph (a), magnification (b), fragmentation (c). C: Endogenous SM expressed as nmol SM per 10^6 cells. [^{14}C]palmitic acid (D) and [^{14}C]serine incorporation (E), expressed as relative percentage of incorporation per 10^6 cells (* $P < 0.05$). F-a: Lytic lysenin activity (final concentration, 5 μM/ml) by different incubation times (10, 30, and 60 min) was measured by the release of LDH. The results are expressed as relative LDH activity respect to 100% value of the cell layer lysed with 0.2% Tween 20. SM distributions using lysenin staining were observed by confocal microscopy optical section and the xz and yz plane reconstruction. Images from a middle confocal plane in both cultured cell conditions (b and c) and z-plane reconstruction (xy and zy) were observed. RT-PCR (G) and qRT-PCR (H) for SMS1 and SMS2 were performed. I: Representative TLC of NBD-SM synthesis in the supernatant and cell. Quantification expressed as relative percentage of optical density (Hyper/Iso per 10^6 cells) (* $P < 0.05$).

for 48 h, they acquired a more packed cobblestone-like morphology, typical of differentiated epithelial cells (Fig. 1A-b). To further determine the SM amount and metabolism in cultured cells, cells were subjected to hypertonicity, and, after extraction, dried lipid extracts were separated by TLC. To confirm its identity, the chromatographic spot corresponding to the Rf of SM was analyzed by mass spectrometry (MALDI TOF/TOF) (Fig. 1B). The intensity versus mass (*m/z*) graph shows most of the signal in the *m/z* 650–850 range (Fig. 1B-a). The magnification of this *m/z* range (Fig. 1B-b) shows peaks of possible subspecies of SM with different fatty acid carbon number. The molecular structures of the SM subspecies were confirmed by fragmentation, with

the detection of a peak at *m/z* 184 corresponding to phosphocholine (Fig. 1B-c).

Thereafter, SM was quantified by the Fiske-Subbarow method. Results are expressed as nmol of SM/10^6 cells. Hypertonicity induced a >2-fold increase in the total endogenous content of SM (Fig. 1C). To determine SM synthesis, cells treated as described above were incubated in the presence of [^{14}C]palmitic acid. As expected, an increase in radioactive SM was obtained under hypertonicity (Fig. 1D). Considering that [^{14}C]palmitic acid can enter the metabolic pathway at different steps, both as substrate of serine palmitoyl transferase (SPT) and as substrate of Cer synthases during de novo synthesis and during the recycling pathway, we further studied [^{14}C]serine incorporation as a reflection of the de novo synthesis pathway. When cells were incubated with [^{14}C]serine, [^{14}C]SM level increased in cells subjected to hypertonicity (Fig. 1E). These results confirm that hypertonicity increases SM cellular content and synthesis.

We further analyzed SM content in PM determining lytic lysenin activity (5 μM/ml) by release of LDH. As expected, the relative LDH release was almost three times higher in cells subjected to hypertonicity than in control cells (Fig. 1F-a).

To determine the cellular SM distribution z-scan of confocal immunofluorescence using lysenin staining was performed. Images from a middle confocal plane show positive fluorescent signal in both cultured cell conditions (Fig. 1F-b, c). In the xz and yz reconstruction, it is observed that while under isotonicity lysenin staining is distributed all over the cells drawing cell periphery (Fig. 1F-b, xz and yz plane, arrowhead), and under hypertonicity most of the signal is basolaterally accumulated (Fig. 1F-c, xz and yz plane, arrowhead). These images of lysenin distribution resemble those reported by Ishitsuka et al. (37) in MDCK cells showing lysenin staining is accumulated in lateral membrane

In order to evaluate the expression of both SMS1 and SMS2 in MDCK cells, we performed an RT-PCR assay. The results showed that both isoforms are expressed in MDCK cells, with the expression of SMS1 lower than that of SMS2 under isotonicity, keeping an SMS2/SMS1 ratio of ∼1.5. When subjected to external hypertonicity for 48 h, the relative expression of SMS mRNA switched, and the SMS2/SMS1 ratio turned to a value <0.75 (Fig. 1G). Then, SMS1 and SMS2 mRNAs were quantitatively analyzed by qRT-PCR. For this purpose, a new set of primers was designed (see Materials and Methods). We compared SMS1 and SMS2 expression in cells cultured either under isotonicity or hypertonicity. Significant increase in SMS1 mRNA was found under hypertonicity while a decrease in SMS2 mRNA was obtained, both normalized by β-actin expression (Fig. 1H). These results show that SMS1 is the prevalent SMS isoform expressed in hypertonicity-induced differentiated MDCK cells.

To evaluate the correlation between SMS1/SMS2 gene expression and the respective enzyme activity, we next determined SMS1 and SMS2 activity by using a protocol that allows discriminating SM synthesis in the Golgi apparatus from SM synthesis in the PM, subjected or not to hypertonicity. For this purpose, treated cells were incubated in the presence of C_6-NBD-Cer at 4°C for 4 h, and then BSA extraction was performed (see Materials and Methods). The SM obtained from the scraped-off cells was considered as the SM pool synthesized in the Golgi apparatus, which corresponds to SMS1 activity (Cell-NBD-SM), whereas the BSA-extracted SM is considered as the SM pool synthesized in the PM and reflects SMS2 activity (Supernatant-NBD-SM). Fig. 1I shows a representative HPTLC obtained from experiments performed in isotonic and hypertonic conditions (cell and supernatant) and a quantification of the spots adjusted to cell number. An HPTLC of different SL standards is also shown (standard). The SM fluorescence intensity of the supernatant extracted from hypertonicity-subjected cells was significantly lower than that extracted from isotonicity-subjected cells (Fig. 1I, Supernatant-NBD-SM, gray bar), denoting a decrease in PM-SMS2 activity. However, the spot corresponding to Golgi SM was higher in hypertonicity-subjected cells (Fig. 1I, Cell-NBD-SM, gray bar). These results suggest that, in cells subjected to hypertonicity, SMS activity in the Golgi apparatus is more relevant than that in PM. These results are consistent with the switch in the expression of SMS genes evoked by external hypertonicity (Fig. 1G, H).

SMS1 knockdown impairs the acquisition of the differentiated phenotype

The above results allow us to consider SMS1 as the most important SMS isoform involved in the progress of hypertonicity-induced MDCK differentiation. To obtain a more precise approach of SMS1 participation during hypertonicity-induced MDCK differentiation, we knocked down SMS1 by the siRNA technique. Silencing of SMS2 and scramble siRNA was also performed as control experiments. The effectiveness and specificity of RNA silencing were analyzed in each case evaluating the expression of SMS1 and SMS2 by RT-PCR. The samples from cultured cells transfected with SMS1 siRNA showed a significant decrease in SMS1 mRNA level as compared with the scrambled-siRNA-treated cells. It is important to note that mRNA SMS2 level did not decrease but appeared moderately increased as compared with the scrambled sample, which may reflect induction of SMS2 mRNA when expression of SMS1 mRNA was knocked down. When SMS2 mRNA was silenced, a moderate decrease in its RNA expression was observed (**Fig. 2A**).

We further determined SMS1 and SMS2 activity by incubation of cultured cells with C_6-NBD-Cer as described above. In the cells treated with SMS1 siRNA, SM synthesis in the Golgi apparatus decreased as compared with treated cells with scrambled siRNA (Fig. 2B), thus reflecting that SMS1 knockdown evoked a decrease in Golgi SM synthesis, demonstrating that the silencing of SMS1-RNA is accompanied by a decrease in SMS1 enzyme activity. No changes in the intracellular synthesis of SM were obtained when cells were transfected with SMS2 siRNA, while synthesis in the PM remained at a very low level.

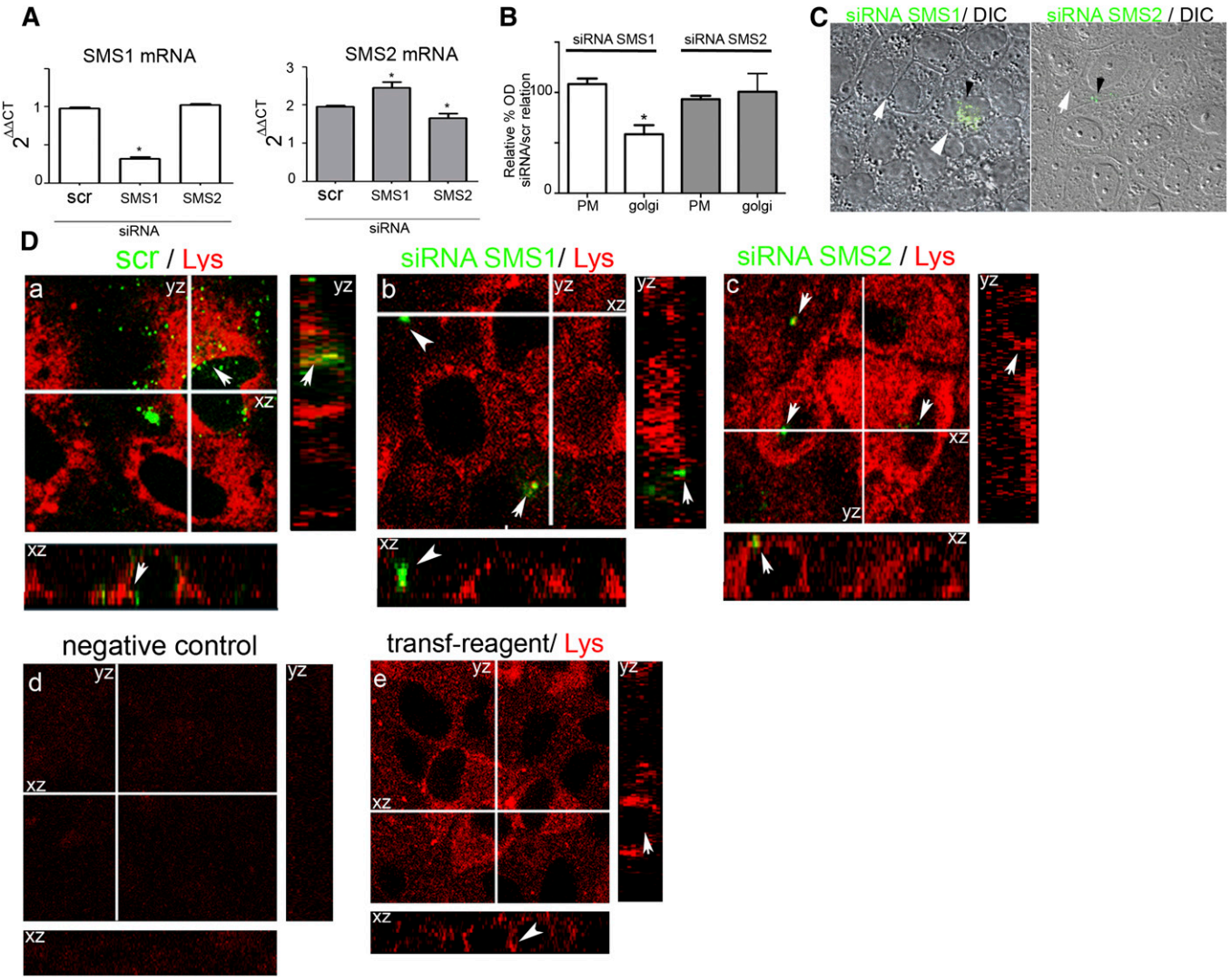

Fig. 2. SMS1 knockdown impairs the acquisition of the differentiated phenotype. A: qRT-PCR analysis of the effect of SMS1 and SMS2 silencing on SMS1 and SMS2 expression. B: Effect of SMS1 and SMS2 silencing on PM and Golgi synthesis of SM expressed as relative percentage of siRNA/scr activity (* $P < 0.05$ data compared by ANOVA). C: DIC of SMS1 and SMS2 siRNA. SMS1-transfected cells (siRNA-Alexafluor488 green dotted cells, arrowhead) and nontransfected cells (white arrow). D: SM distributions using lysenin staining were observed by confocal microscopy optical section and the xz and yz plane reconstruction. Images from a middle confocal plane and z-plane reconstruction (xy and zy) in siRNA scramble (a), siRNA SMS1 (b), and siRNA SMS2 (c) transfected cells were observed. Negative control (avoiding lysenin) (d) and transfection reagent control (e) were performed.

To evaluate the effect of SMSs knockdown on transfected cells, immunofluorescence microscopy was performed. Negative-siRNA conjugated with Alexafluor488 was used as control of cotransfection. The cells transfected with SMS siRNAs presented a green dotted signal in the cytoplasm (Fig. 2C, small arrowhead). Morphological changes were determined by DIC microscopy. SMS1 siRNA-Alexa488-positive cells presented loss of the hexagonal phenotype and more diffuse cell-cell limits (Fig. 2C, arrowhead) when compared with nontransfected cells (Fig. 2C, arrow). By contrast, no changes in the cell phenotype were observed in SMS2 siRNA-transfected cells.

Quantitative data showed that 75% of scrambled cells or those transfected with siSMS2 had conserved phenotype while the 85% of cells transfected with siSMS1 presented altered phenotype.

We further evaluated the level and distribution of SM by lysenin staining. In the middle plane of Fig. 2D-a, it can be observed that cytosolic labeling of SM may be due to binding of lysenin to intracellular vesicles, which was attenuated by SMS1 (Fig. 2D-b) but not by SMS2 silencing (Fig. 2D-c). As shown in z reconstruction, SMS1 silencing evoked a lysenin signal dissipation from the basolateral domain (arrowhead and arrow), while no change was observed in SMS2 siRNA (Fig. 2D-b) if compared with scramble-transfected cells (Fig. 2D-a) and cells treated with the transfection reagent alone (Fig. 2D-e). No fluorescent signal was observed in cells incubated without lysenin (Fig. 2D-d).

Taken together, the results suggest that SMS1 activity is important for the maintenance of cell-cell adhesion and for cells to develop the differentiated morphology.

JOURNAL OF LIPID RESEARCH ASBMB

The morphological changes induced by hypertonicity are impaired by an SMS inhibitor in a concentration-dependent manner

As described above, SMS1 knockdown impaired hypertonicity-induced MDCK differentiation. To obtain more evidence and to allow the progressiveness of this process, we performed experiments with increasing concentrations of an SMS inhibitor (D609). To select the optimal D609 concentration, we first determined cell number and cell viability (**Fig. 3A**, B) and found no differences from 7.5 to 15 μM D609 but a toxic effect at 20 μM D609, reflected by a significant decrease in cell number and viability.

Because D609 is an inhibitor of SMSs and SM is a final product of SL metabolism, we further determined the SM amount and metabolism in cultured cells treated or not with D609. To this end, cultured cells were subjected to hypertonicity, and, after extraction, dried lipid extracts were subjected to TLC. Thereafter, the chromatographic spots corresponding to the Rf of SM were quantified by Fiske-Subbarow. Results are expressed as nmol of SM/10^6 cells. As expected, when cultured cells were treated with increasing concentrations of D609, the endogenous level of SM decreased in a concentration-dependent manner (Fig. 3C, gray bars). We further studied [^{14}C]serine incorporation as a reflection of the de novo synthesis pathway. When cells were incubated with [^{14}C]serine, the serine incorporation to SM decreased as compared with the control at any of the inhibitor

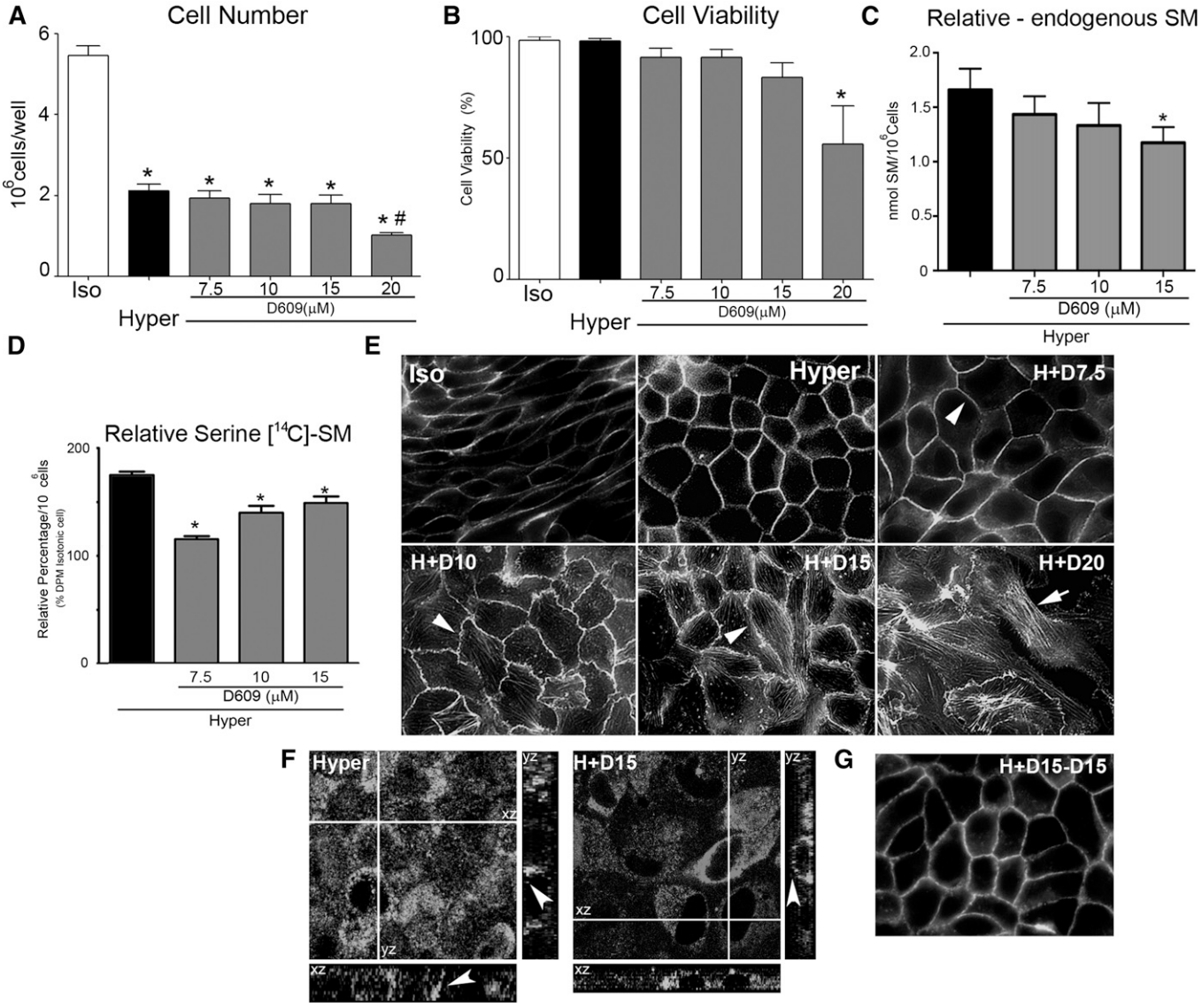

Fig. 3. The morphological changes induced by hypertonicity are impaired by D609, an SMS inhibitor, in a concentration-dependent manner. Effect of increasing concentrations of D609 on cell number (A) and viability (B) (* $P < 0.01$ data compared vs. Iso; # $P < 0.05$ data compared vs. Hyper). C: Effect of increasing concentrations of D609 on the endogenous levels of SM expressed as nmol of SM per 10^6 cells (* $P < 0.05$). D: Effect of increasing concentrations of D609 on SM de novo synthesis (* $P < 0.05$). E: Wide-field fluorescence microscopy showing the effect of increasing concentrations of D609 on cell morphology. F: Lysenin staining of SM in control (Hyper) and D609 treated cells (H+D15). G: Washed cells reincubated for 24 h without inhibitor.

concentrations used, thus reflecting inhibition of SM de novo synthesis (Fig. 3D)

We further studied the effect of D609 on the MDCK cell phenotype by wide-field fluorescence microscopy. Changes in cell shape were observed by visualization of phalloidin-FITC fluorescence, where its peripheral distribution reflects the presence of polymerized actin forming the cell cortex. Confluent MDCK cells cultured in isotonic medium displayed an elongated fibroblast-like phenotype, whereas those cultured in hypertonic medium for 48 h acquired a more packed cobblestone-like morphology, typical of differentiated epithelial cells (Fig. 3E).

To determine whether inhibition of SMS can affect the hypertonicity-induced epithelial phenotype, cultured cells were treated with increasing concentrations of D609. At 7.5 μM D609, most of the cells kept their differentiated phenotype with actin distributed in the cell cortex (Fig. 3E, H+D7.5, arrowhead). As D609 concentration increased, alterations in cell-cell contacts were evident, and the cell limits became irregular. At 10 μM D609, the cell borders acquired a zipper-like appearance, and stress fiber formation was evident (Fig. 3E, H+D10, arrowhead). At 15 μM D609 (Fig. 3E, H+D15), the F-actin cell cortex was more disrupted, with alteration of the points of cell-cell adhesion (arrowhead). At 20 μM D609, the F-actin cell cortex was lost in most of the cells, and F-actin organized as intracellular parallel fibers that do not correspond to an epithelial cell phenotype (Fig. 3E, H+D20, arrow) but resemble a fibroblast-like phenotype.

To determine the effect of D609 in the cellular distribution of SM, z-reconstruction of confocal immunofluorescence using lysenin staining was performed. Images from a middle confocal plane show cytosolic labeling of SM may be due to binding of lysenin to intracellular vesicles, which was attenuated by D609-treated cells (Fig. 3F, H+D15). In the xz and yz reconstructions, it is observed that under hypertonicity most of the signal is basolaterally accumulated (Fig. 3F, Hyper, arrowhead) while in D609-treated cells lysenin staining is distributed all over the cells drawing cell periphery (Fig.3F, H+D15, arrowhead).

In order to evaluate the reversibility of the D609 effect, cultured cells were washed and incubated for another 24 h in the absence of the inhibitor. Results show that cells recovered their differentiated phenotype, thus demonstrating no deleterious effect of D609 (Fig. 3G).

SMS inhibition and SMS1 knockdown impair AJ assembly: alteration of E-cadherin

Being that AJ is the most important cell-cell adhesion structure and considering that it is initiated by the homophilic interaction of E-cadherin of adjacent cells, we next studied E-cadherin distribution by confocal immunofluorescence. We evaluated SMS involvement by two strategies: the pharmacological inhibition of the enzyme activity and SMS1 knockdown. The images of the middle confocal plane are shown in **Fig. 4**. Under isotonicity, E-cadherin appeared retained in cell-cell adhesions, showing the fibroblast-like phenotype (Fig. 4A-a, d), whereas under external hypertonicity for 48 h, E-cadherin perfectly delineated the square shape, typical of the differentiated phenotype displayed by MDCK cells (Fig. 4A-b, e). When cells were treated with 15 μM D609, E-cadherin positive signal in cell-cell junctions was lost in most of the cells (Fig. 4A-c, f). Instead of continuous peripheral distribution, E-cadherin showed a discontinued distribution, acquiring a dot-like appearance (Fig. 4A-c), better observed in the magnified image (Fig. 4A-f, arrowheads). The dissipation of E-cadherin immunofluorescence was further corroborated by Western blot analysis. Indeed, the positive signal for E-cadherin progressively decreased as D609 concentration increased (Fig. 4B).

To confirm SMS1 involvement in AJ alteration, E-cadherin distribution was also evaluated in SMS1 or SMS2 knockdown cells. As seen in Fig. 4C, SMS1 siRNA-transfected cells (small arrowhead) presented discontinuous PM E-cadherin distribution, with a clear loss in the periphery of the cell (Fig. 4C, white arrowhead) as compared with nontransfected cells (Fig. 4C, white arrow). No alteration in E-cadherin distribution was observed in SMS2 siRNA-transfected cells (Fig. 4D).

SMS inhibition and SMS1 knockdown impair AJ assembly: alteration of α- and β-catenin

It is considered that the stabilization of the cell-cell adhesion properties of E-cadherin depends on the cytoplasmic domain. In fact, to exhibit stable functional adhesion, E-cadherin must form complexes with cytoplasmic plaque proteins called catenins and with the actin cytoskeleton. The cytoplasmic E-cadherin domain binds β-catenin, which in turn binds α-catenin, which connects with the actin cytoskeleton. Thereafter, we analyzed the role of SMS in the correct distribution of β- and α-catenin by the pharmacological inhibition (**Fig. 5A**) and the knockdown of SMS1 (Fig. 5C, D). Both β- and α-catenin were found in the periphery of the cells, both under isotonicity and under hypertonicity for 48 h (Fig. 5A-a, g/b, h, respectively). However, merged images showed better colocalization of β- and α-catenin in cells subjected to hypertonicity than in those in isotonicity (Fig. 5A-m, n, respectively), reflecting maturation of cell-cell adhesions induced by hypertonicity. The magnified images allowed us to observe the typical organized rows of puncta at sites of cell-cell contact in cells under isotonicity. After 48 h of hypertonicity, the puncta increased in number and size and appeared to fuse until constituting a continuous line formed by a single highly organized row of puncta, typical of mature AJs (Fig. 5A-s, ´s/t, ´t) (38). When cultured cells were treated with increasing concentrations of D609, the typical epithelial sheet was increasingly altered. In fact, at 7.5 μM D609, cell-cell adhesion started to be impaired and some cells acquired an elongated fibroblastic phenotype (Fig. 5A-c, i, and o). In the magnified image, it is possible to see that the positive signal for α- and β-catenin appeared as two distinct rows of puncta at sites of intercellular contact (Fig. 5A-u, arrowhead), losing the continuous line of colocalized β- and α-catenin (Fig. 5A-´u). At 10 μM D609, the effect of the inhibition of SMSs was more evident (Fig. 5A-d, j, and p), cell-cell adhesion was impaired in most of the

JOURNAL OF LIPID RESEARCH ASBMB

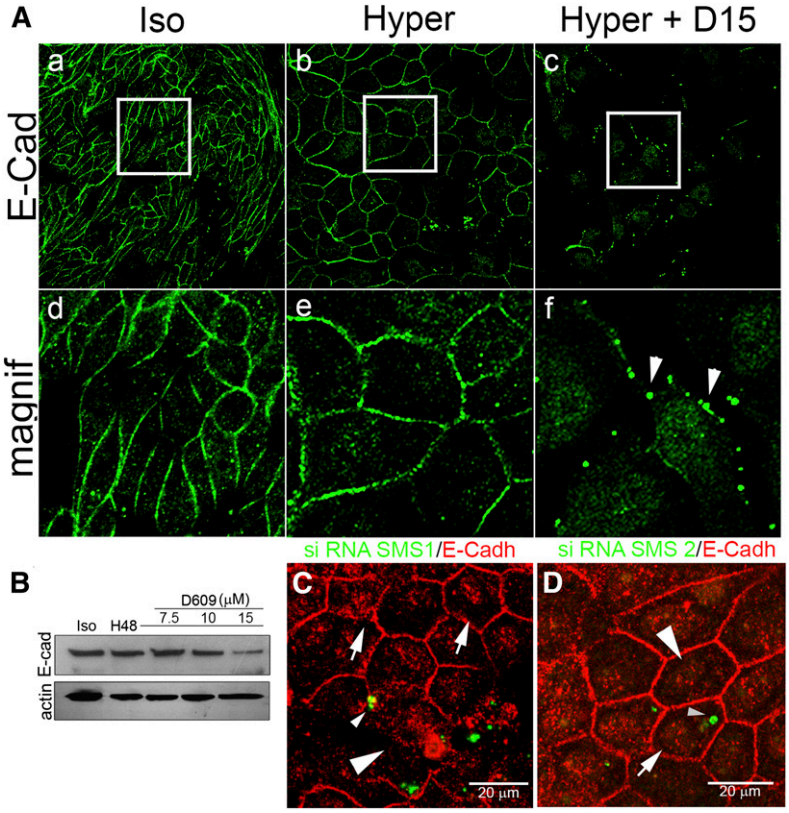

Fig. 4. SMS inhibition and SMS1 knockdown impair AJ assembly: alteration of E-cadherin. A: E-cadherin (green fluorescence) images of the middle confocal plane and their magnification under isotonicity (a and d), hypertonicity (b and e), and under hypertonicity with 15 μM D609 (c and f). B: Effect of increasing concentrations of D609 on E-cadherin level. C: Immunofluorescence of E-cadherin distribution in SMS1 knockdown transfected cells (small arrowhead) as compared with nontransfected cells (white arrowhead). D: Immunofluorescence of E-cadherin distribution in SMS2 knockdown transfected cells (small arrowhead) compared with nontransfected cells (white arrowhead).

cells, and the dissipation of the α/β-catenin signals was evident in some zones of the cell culture [Fig. 5A-v (arrowhead), ´v]. At 15 μM D609, cell-cell adhesion was also impaired in most of the cells, with a complete dissipation of the α/β-catenin signals in some zones [Fig. 5A-w, ´w (arrowhead)]. At 20 μM D609, cells lost their epithelial phenotype, cell-cell adhesions were disrupted, and cells appeared completely irregular (Fig. 5A-f, l, and r). Some cells developed a pseudopod-like structure (Fig. 5A-r, arrow), and most of the cells showed α/β-catenin-labeled filopodium-like structures to contact each other (Fig. 5A-x, arrowhead). In these conditions the α/β-catenin puncta were smaller, although organized in the periphery of the cells, but appeared to serve as points where filopodia emerge punctuate and embedded into neighboring cells (Fig. 5A-´x). It is interesting to note that β-catenin was present in the cytoplasm, which seems to reflect a cytoplasmic translocation of the protein evoked by the treatment with 20 μM D609 (Fig. 5A-l, arrowhead). In some cells, intranuclear β-catenin was also observed.

In order to evaluate the reversibility of the D609 effect, cultured cells treated with 15 μM D609 were washed and reincubated without inhibitor during additional 24 h. As is seen in the merged image (Fig. 5B), AJ recovered their mature phenotype.

It is accepted that cells require the constant expression and function of AJ proteins to remain associated and organized as an epithelium (38). Furthermore, for cadherins to exhibit functional adhesion activity, they must form complexes with the cytoplasmic plaque proteins α- and β-catenins. Because β-catenin is a necessary intermediate in the linkage of α-catenin to the cadherin cytoplasmic domain, we performed Western blot analysis to address the presence of α- and β-catenin. α-catenin was highly sensitive to the increasing concentration of D609, showing an important decrease in the amount of protein from 7.5 μM D609 (Fig. 5C, white bars). β-catenin appeared more resistant to the effect of D609, but at 15 μM a decreased amount of the protein was evident (Fig. 5C, gray bars).

To confirm the progressive effect of the inhibitor, SMS1 knockdown experiments were performed. When α-catenin distribution was evaluated, we observed that SMS siRNA-transfected cells (Fig. 5D, α-catenin, white arrow) presented a diffuse disrupted signal in the PM (Fig. 5D, α-catenin, white arrowhead) compared with nontransfected cells (Fig. 5D, α-catenin, small arrowhead). Only the cell-cell contact of cells adjacent to positively transfected but not to nontransfected cells presented a dissipation of the α-catenin signal in the cell periphery. These results show that SMS1 knockdown alters α-catenin distribution. When β-catenin distribution was evaluated, the immunofluorescence images showed that SMS1 siRNA-transfected cells presented a wider, more diffuse β-catenin distribution in the periphery of the cells with evident signals of cell-cell adhesion relaxation (Fig. 5D, β-catenin, white arrows) compared with nontransfected cells (Fig. 5D, small arrowheads). These results show that SMS1 silencing evokes an impairment of cell-cell adhesion integrity, suggesting an important role of SMS1 in AJ conformation. Additionally, transfected cells (green dotted

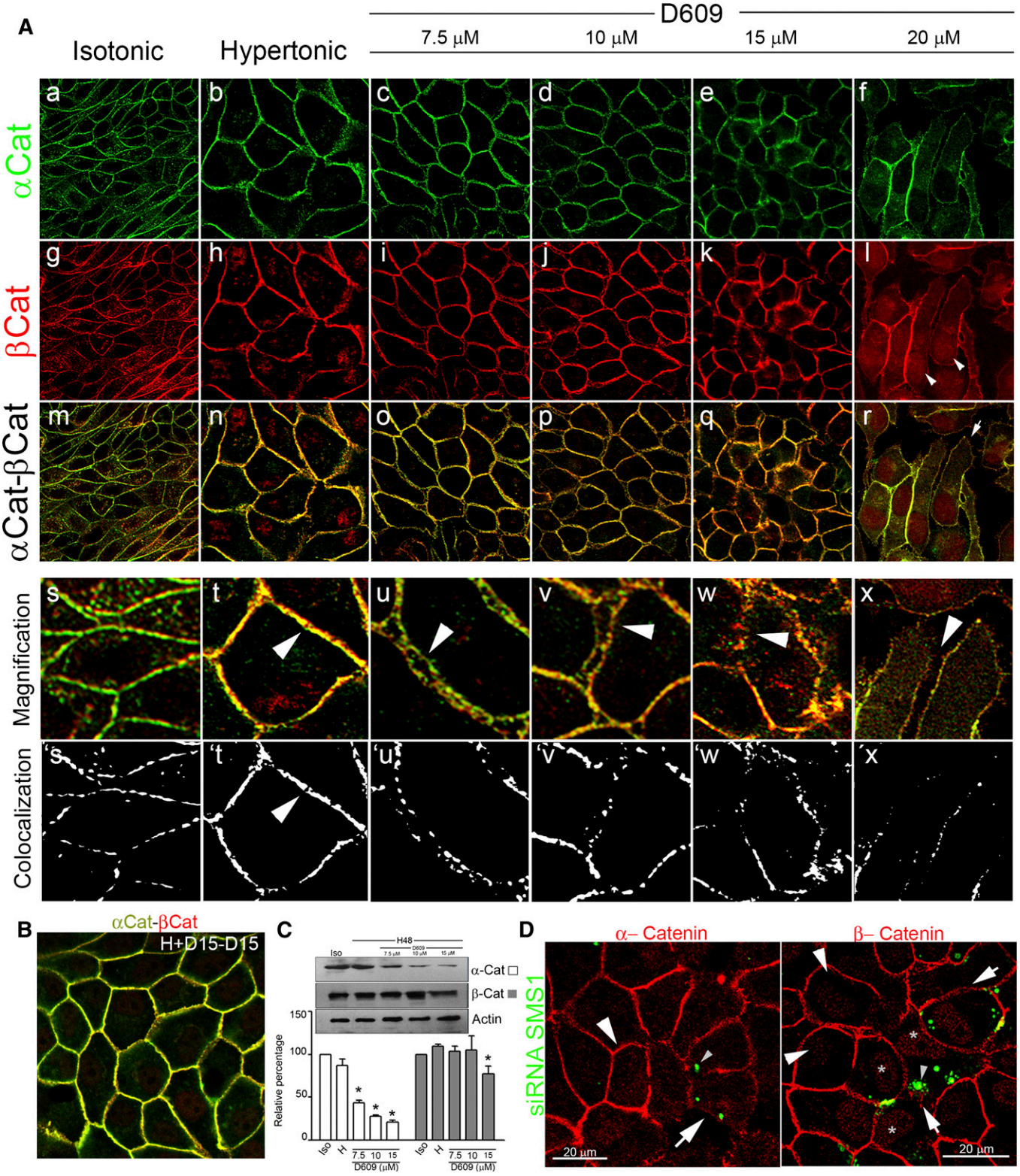

Fig. 5. SMS inhibition and SMS1 knockdown impair AJ assembly: alteration of α- and β-catenin. A: Confocal immunofluorescence of the middle confocal plane of α-catenin (α-Cat) and β-catenin (β-Cat) distribution, under isotonic (a, g, respectively) or hypertonic conditions (b, h, respectively). Merged images (m, n). Confocal immunofluorescence of the middle confocal plane of α-catenin (c–f) and β-catenin distribution (i–l). Merged images of β- and α-catenin (o–r). Digital magnification (s–x). Arrowheads show the progressive alteration of AJ and cell-cell adhesion. From magnified images, segmentation processes were performed. Yellow pixels are represented as white pixels (Colocalization: s´, t´, u´, v´, w´, and x´). B: α-catenin (green) and β-catenin (red) were detected in wash cultured cells and reincubated without inhibitor. C: Effect of increasing concentrations of D609 on α-catenin (white bars) and β-catenin (gray bars) levels determined by Western blot analysis. Actin was used as loading control (representative image, n = 4, $P < 0.05$). D: Effect of SMS1 knockdown on α-catenin (red) and β-catenin (red) distribution. Transfected cells are seen as green dotted cells (small arrowhead).

JOURNAL OF LIPID RESEARCH ASBMB

cells, small arrowhead) presented a β-catenin cytoplasmic distribution consistent with the effect observed with the highest D609 concentration (Fig. 5D, gray "*").

To obtain additional support for the observation that hypertonicity induces the maturation of AJs, we analyzed the cell-cell adhesion structure through serial z-axis 0.5 μm optical sections on cells subjected to isotonicity and hypertonicity either with or without D609 15 μM treatment (**Fig. 6A**). We generated z-plane cross-sections across the monolayer (Fig. 6A, lines a–d). Analysis of z-planes (Fig. 6A, Z Plane) showed β- and α-catenin (red and green fluorescence, respectively) in the periphery of the cells, both under isotonicity and under hypertonicity (Fig. 6A, Isotonic, Z Plane, white arrowheads). However, images showed that cells subjected to hypertonicity presented better colocalization of β- and α-catenin than cells maintained under isotonicity. When cultured cells were treated with D609, cell-cell adhesion was impaired and the peripheral localization of α- and β-catenin was lost, reflecting cell-cell adhesion disruption (Fig. 6A, Hyper + D15, white arrow).

To obtain a closer examination of the cell morphology, 3D reconstructions were performed from the optical

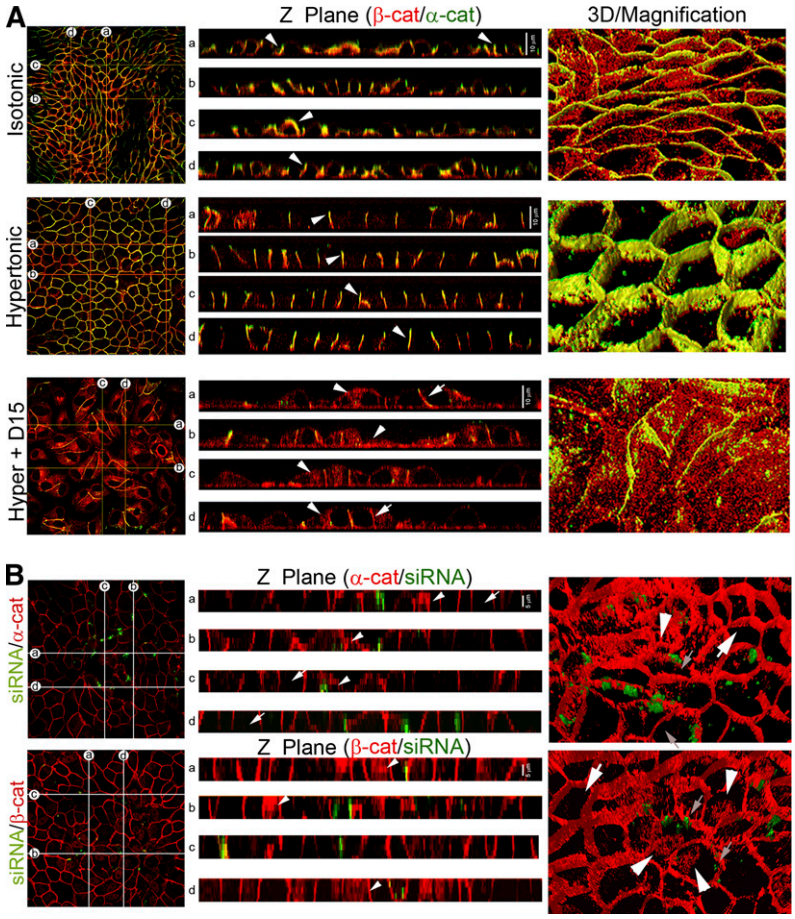

Fig. 6. Z-plane and 3D reconstruction. SMS inhibition and knockdown. A: Z-plane cross-sections across the monolayer were generated (a–d). Analysis of z-planes (Z Plane) showed β- and α-catenin in the periphery of the cells, both under isotonicity and under hypertonicity (white arrowhead). In cells treated with 15 μM D609, cell-cell adhesion was impaired and the peripheral localization of α- and β-catenin is lost (Hyper+D15, white arrow). Cytosolic β-catenin was observed (Hyper+D15, white arrowhead). 3D reconstructions were performed from the optical sections (3D/Magnification). Under isotonicity, cells presented an elongated phenotype while under hypertonicity presented a cobblestone-like morphology (Hypertonic, 3D/Magnification). D609 treatment impaired the acquisition of the differentiated phenotype (Hyper + D15, 3D/Magnification), showing β-catenin intracellular accumulation. B: Effect of SMS1 knockdown on AJ formation and cell morphology, α- and β-catenin (red fluorescence in both cases). The green fluorescence corresponded to transfection control. Analysis of z-planes (Z Plane, α-cat and β-cat) showed that images from transfected cells (arrowhead) present a mislocalization of both catenins, with a clear cytoplasmic β-catenin distribution (Z Plane, β-cat, arrowhead). No alteration is observed in nontransfected cells, which present a cobblestone-like phenotype, with β-catenin peripherally distributed (white arrow). In α-catenin 3D/Magnification nontransfected cells (white arrow) present a peripheral distribution of α-catenin, whereas peripheral distribution is disrupted in transfected cells. In β-catenin 3D/Magnification nontransfected cells showed a peripheral distribution (white arrow), whereas transfected cells (white arrowhead) present intracellular distribution with accumulation in a structure that should be the nucleus. The small arrowhead indicates the transfection control.

sections (Fig. 6A, 3D/Magnification). This approach allowed observing that under isotonic conditions, cells presented an elongated phenotype with a lower height than under hypertonic conditions. Moreover, cells under hypertonic conditions presented a perfect cobblestone-like morphology, typical of the differentiated epithelial cell phenotype (Fig. 6A, Hypertonic, 3D/Magnification). The treatment with D609 impaired the acquisition of such differentiated phenotype (Fig. 6A, Hyper + D15, 3D/Magnification), showing intracellular accumulation of β-catenin.

To confirm the effect of SMS1 knockdown on AJ formation and cell morphology, α- and β-catenin (red fluorescence in both cases) distribution was analyzed. The green fluorescence corresponded to negative-siRNA-Alexafluor488 cotransfection control. Analysis of z-planes (Fig. 6B, Z Plane, α- and β-cat) showed that α- and β-catenin in the periphery of the cells. However, images showed that transfected cells (arrowheads) presented a mislocalization of both catenins, with a clear cytoplasmic β-catenin distribution (Fig. 6B, Z Plane, β-cat, arrowhead). These effects were better observed in 3D reconstruction. As seen in Fig. 6B (α-cat, 3D/Magnification), cells presented an elongated morphology with alteration in the peripheral distribution of α-catenin (white arrowhead) when compared with nontransfected cells (white arrow). In Fig. 6B (β-cat, 3D/Magnification), the transfected cells (small arrow) present dissipation of β-catenin from cellular borders, with intracellular accumulations (white arrowhead). No alteration was observed in nontransfected cells, which presented a cobblestone-like phenotype, with β-catenin peripherally distributed (white arrow).

The alteration in the acquisition of the differentiated phenotype by SMS inhibition is not due to Cer accumulation

To study Cer, GlcCer, and LacCer, we developed a two-solvent TLC to resolve them. We first used a butanol-acetic acid-water (60:20:20, v/v/v) system. This TLC was able to resolve LacCer but not Cer or GlcCer, which comigrated with the solvent front (**Fig. 7A**-1). To separate Cer from GlcCer, we cut the TLC plate over the sphingosine standard (corresponding to Rf = 0.8), and a second solvent system was used (chloroform-methanol, 98:2, v/v). This allowed us to resolve Cer and GlcCer (Fig. 7A-2). To confirm the identity of Cer and GlcCer, the chromatographic spots that comigrated with Cer and GlcCer standards were analyzed by mass spectrometry (MALDI TOF/TOF). The intensity versus mass (*m/z*) graph shows most of the signal in the *m/z* 520–690 range. These *m/z* peaks were consistent with the possible Cer subspecies (different fatty acid carbon number) (Fig. 7B). The molecular structures of these Cer subspecies were confirmed by fragmentation, with the detection of two peaks at *m/z* 282.3 and 264.3, corresponding to simple and double dehydrated sphingosine, respectively (Fig. 7B, Fragmentation), confirming Cer identity. The same procedure was performed with GlcCer, confirming the different subspecies (Fig. 7C, *m/z* 682–808). Fragmentation rendered three peaks corresponding to double dehydrated sphingosine (*m/z* 264.3), GlcCer-(Glc + $2H_2O$), and GlcCer-(Glc + H_2O), confirming GlcCer identity (Fig. 7C, Fragmentation). In this solvent system, the SM spot was contaminated by lysophosphatidylcholine (confirmed by mass spectrometry, data not shown). For this reason, SM was not considered for this analysis.

To determine whether SMS inhibition induced Cer accumulation that could be involved in the D609-induced morphological changes in the MDCK cell phenotype, cells were treated with D609, and Cer and GlcCer levels were analyzed by [^{14}C]serine incorporation. SMS inhibition showed an increase in [^{14}C]Cer-serine incorporation and a more important increase in GlcCer synthesis (40%) (Fig. 7D, Hyper and H+D15). To evaluate whether such increase in Cer and/or GlcCer synthesis were involved in phenotype alteration, we used Myr, an SPT inhibitor, to avoid the de novo Cer and GlcCer synthesis. Myr treatment inhibited the increase in Cer and GlcCer synthesis (Fig. 7D, H+D15+Myr) induced by SMS inhibition. A change in the endogenous content of Cer was further evaluated by using cupric acetate reagent. Increase in Cer content was observed when cells were treated with D609, which was abolished by addition of Myr. To determine whether Cer and GlcCer accumulation was the cause of phenotype alteration, we performed an indirect immunofluorescence experiment. The alteration in the actin cortex and stress fiber formation induced by SMS inhibition (Fig. 7F, H+D15) was not reversed by Myr treatment (Fig. 7F, H+D15+Myr). Moreover, when we evaluated α- and β-catenin distribution, we observed that the AJ impairment evoked by SMS inhibition was not reversed by Myr treatment (Fig. 7F, H+D15+Myr). We performed the experiment with D-PDMP, a GlcCer synthase-specific inhibitor. D-PDMP inhibited GlcCer synthesis but was not able to reverse the effect of SMS inhibition (Fig. 7F, H+D15+PDMP). We also evaluated the effect of D-PDMP and Myr without the addition of D609. Neither D-PDMP nor Myr caused impairment of AJ stabilization by themselves.

These results show that, in these experimental conditions, SMS inhibition induced a small Cer accumulation and a greater GlcCer accumulation, probably due to the ability of MDCK cells to synthesize GlcCer. In fact, we have previously described that GlcCer synthase activity is increased in MDCK cells subjected to hypertonic stress. The increase in GlcCer synthesis was necessary to acquire apical membrane maturation (25). For this reason, we suggest that the loss of AJ formation by SMS inhibition was due to a decrease in SM level and not to an increase in Cer and/or GlcCer levels.

DISCUSSION

The AJ is the prominent cell-cell adhesion structure in epithelial tissue. Several lines of evidence have demonstrated the involvement of different proteins in the formation and stabilization of AJ (39). However, the importance of membrane lipids in such process has been less studied. In the present study, we demonstrated that the acquisition

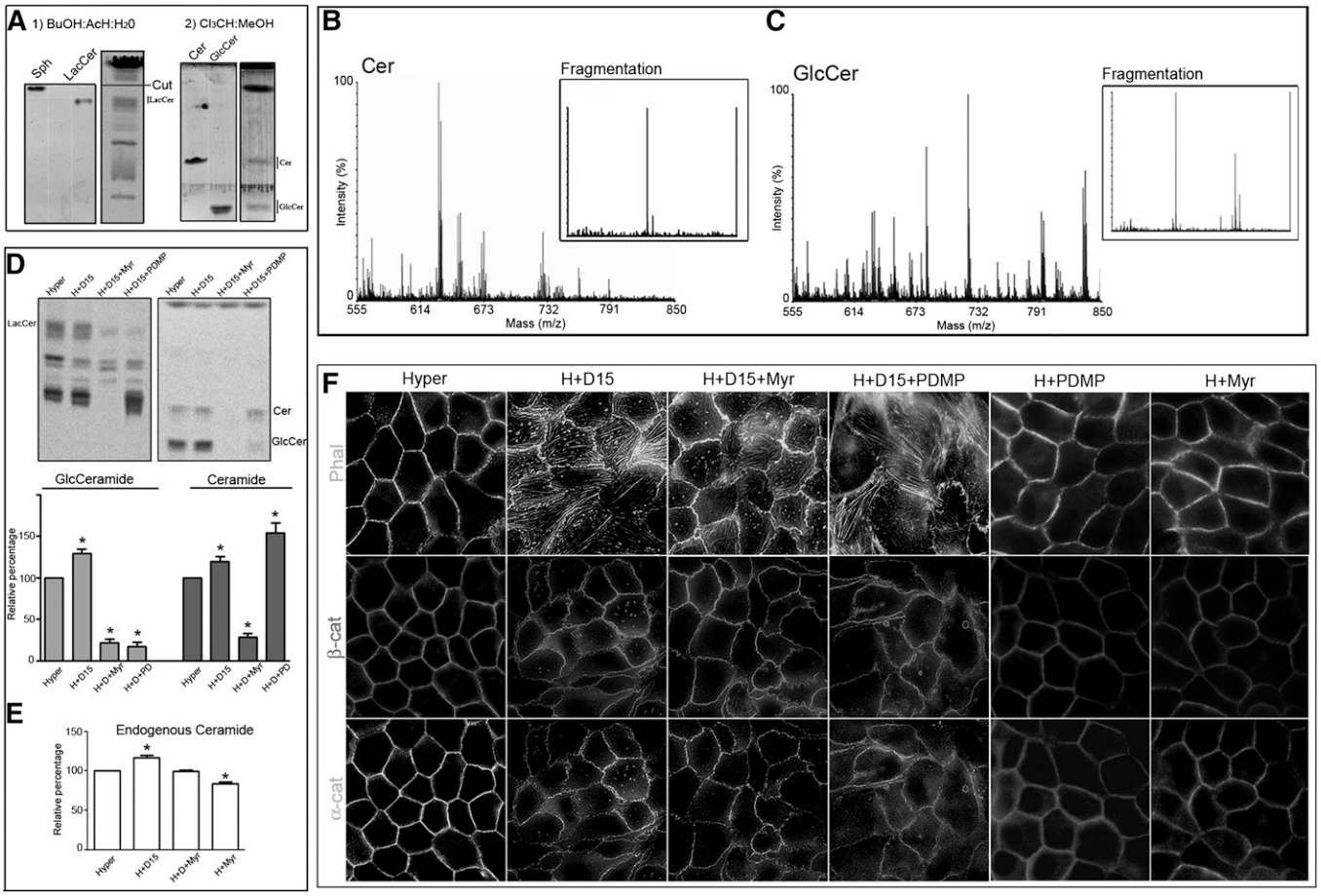

Fig. 7. The alteration in differentiated phenotype acquisition by SMS inhibition is not due to Cer accumulation. A: Representative TLC performed as described in Materials and Methods, using butanol-acetic acid-water (60:20:20, v/v/v) as first solvent system and chloroform-methanol (98:2, v/v) as second solvent system. B, C: MALDI TOF/TOF mass spectrometry of chromatographic spots that comigrated with Cer and GlcCer standards. The intensity versus mass (*m/z*) graph shows most of the signals in the *m/z* 520–690 range in the Cer spot and signals in the *m/z* 682–808 range in the GlcCer spot. These *m/z* peaks are consistent with the possible Cer and GlcCer subspecies (different fatty acid carbon number). The molecular structures of Cer and GlcCer subspecies were confirmed by fragmentation, with the detection of two peaks at *m/z* for Cer and three peaks for GlcCer confirming their identities. D: Effect of SPT and GlcCer synthase inhibition on [^{14}C] serine incorporation, in D609-treated cells. E: Endogenous content of Cer evaluated by cupric acetate reagent. F: Effect of SPT and GlcCer synthase inhibition on the D609-induced alteration of F-actin and α- and β-catenin (α-cat/β-cat) distributions.

of mature AJ structures require active intracellular synthesis of SM, and that when this is affected, AJ cannot be assembled and cells progress to the acquisition of a less mature phenotype.

It is accepted that, to become organized as epithelial tissue, cells have to develop mature cell-cell junctions and acquire a differentiated phenotype. We have previously demonstrated that even after 72 h at confluence, MDCK cells are only partially polarized and that they reach the fully differentiated phenotype after 48 h of external hypertonicity (25). Consistently, in the present study, we showed that after 48 h of confluence, MDCK cells keep an immature fibroblast-like phenotype, but when subjected to 48 h of hypertonicity, they develop a cobblestone-like phenotype typical of mature epithelial cells. In parallel to the acquisition of a mature morphology, cell-cell contact becomes tighter and more stable, reflected by the better colocalization of AJ proteins. In agreement with this, Vasioukhin et al. (39) reported that even at confluence, intercellular adhesion does not reach the stage of mature AJ, but cells are in the stage of passive contacting cell membranes. In our system, mature AJs are obtained after 48 h of hypertonicity, when cells acquire typical epithelial cell morphology.

It has been proposed that the formation of mature AJ is a stepwise process. In the starting step, cells connect to each other by establishing contacting filopodia. This is followed by an intermediate stage where AJ proteins show a double row of puncta, to form a zipper-like structure with undulated intercellular borders. Thereafter, a well-defined simple row of puncta with parallel actin filaments appears (40). Based on this stepwise model of AJ maturation, our results seem to show that as the inhibition of SM synthesis increases, the capacity of MDCK cells to obtain established AJ decreases. In fact, at 20 μM D609, MDCK cells only reach the starting stage of adhesion because only contacting filopodia are present. At lower concentrations of the inhibitor (10 μM), cell-cell contacts stop at the stage of separated double row of puncta and become closer at the lowest concentration of the inhibitor. These results

suggest that, depending on the degree of inhibition, the inhibition of SM synthesis induces weakness and/or blockage of AJ formation.

The alteration in AJ constitution caused by inhibition of SM synthesis also resembles the process of induced AJ disintegration described in MDCK cells by Palovuori et al. (41). By using src-transformed MDCK cells, they demonstrated that the activation of scr evokes the release of AJ components from the lateral cells with the simultaneous vanishing of membranous actin and appearance of large actin bundles. In the present study, we observed almost the same. In fact, as D609 concentration increased, membranous actin fibers were increasingly disorganized until they vanished at 20 μM of the inhibitor to form intracellular large bundles of actin fibers. Together with AJ impairment, increasing inhibition of SM synthesis evoked a decrease in the AJ proteins E-cadherin, β-catenin, and α-catenin. Interestingly, while the lowest concentration of inhibitor did not affect E-cadherin and β-catenin, it decreased α-catenin (Fig. 5B). It is known that actin polymerization at the site of AJs plays a key role during both AJ formation and strengthening (42). Because of the physical association of α-catenin with actin filament, the higher sensitivity of α-catenin to the inhibition of SM synthesis could explain the early weakness of AJs observed at 7.5 μM D609 (Fig. 5).

E-cadherin plays a pivotal role in AJ formation and in establishing and maintaining epithelial cells (43, 44). Because AJ is an E-cadherin-based structure and E-cadherin is a transmembrane protein, it seems obvious to think that among the different SM pools, the PM-synthesized pool is the most involved. However, our results suggest that the pool of SM involved in AJ formation/maturation is of intracellular origin and is SMS1 dependent. Various lines of evidence support these conclusions. First, hypertonicity-induced MDCK cell differentiation is accompanied by an increase in SL de novo synthesis, as reflected by the increase in endogenous SM and [^{14}C]SM (with serine and palmitic acid precursors, Fig. 1C–E). Second, while SMS1 expression increases, SMS2 expression decreases during differentiation (Fig. 1G, H). Third, by using the experimental protocol developed by van Helvoort et al. (35) and modified by Ternes et al. (36), we observed a selective increase in intracellular SM synthesis when cells were subjected to a hypertonic medium. The fact that SMS1 is of Golgi but not PM localization permits us to suggest that SMS1 but not SMS2 is the enzyme involved in MDCK cell differentiation and AJ conformation. These observations are in agreement with the decrease observed in the endogenous amount of SM produced by D609 because, as reported by others, the endogenous mass of SM is mostly dependent on SMS1 activity (6). Moreover, we determined that SMS1 was the isoform more affected by the D609 concentration used (data not shown). We further confirmed the involvement of SMS1 by the experiments using siRNA SMS1 because the decrease in SMS1 mRNA was accompanied by a decrease in Golgi SM (but not in PM SM) synthesis and impairment of AJ establishment.

Inherently, we observed that SMS inhibition induced an increase in GlcCer synthesis. The possible explanation for this was that, in our experimental conditions, MDCK cells were able to use the excess of Cer to form GlcCer. In fact, we have previously described that GlcCer synthase activity increased in MDCK cells and was necessary for apical membrane establishment during differentiation (25). It is important to note that despite the importance of GlcCer in the differentiation process, the SM levels have to be maintained for correct AJ formation.

At this point, we can assume that SMS1 activity is a requirement for the maintenance and maturation of cell-cell adhesion. It is known that AJ is in continuous recycling of E-cadherin. Thus, the efficient delivery of E-cadherin to the lateral cell membrane is critical for AJ preservation in polarized cells (45, 46). Different lines of evidence support our results. The downregulation of SMSs in the Golgi apparatus retards the protein from the trans-Golgi network to the PM (8). Additionally, it has been shown in HeLa cells that E-cadherin exits the Golgi apparatus and reaches the PM by a recycling endosomal pathway (47). On the other hand, Gagescu et al. (48) reported that recycling endosomes are rich in SM and cholesterol and that this lipid-based sorting mechanism contributes to the maintenance of cell polarity. More recently, Yachi et al. (49) demonstrated that SMS1 is the main enzyme responsible for the generation of recycling endosomes of SM. All these observations and our present results allow us to suggest that active SMS1-dependent synthesis of SM is necessary to establish mature AJs due to the fact that SM could be essential to form the intracellular vesicles involved in the correct delivery of AJ proteins.

In conclusion, the present results suggest a new role for the intracellular synthesis of SM as a requirement for the establishment of mature AJs, thus emerging as a relevant player in the acquisition of the differentiated epithelial cell phenotype.

The authors thank Roberto Fernández for confocal microscope technical assistance.

REFERENCES

1. Ogretmen, B., and Y. A. Hannun. 2004. Biologically active sphingolipids in cancer pathogenesis and treatment. *Nat. Rev. Cancer.* **4:** 604–616.
2. van Echten, G., R. Birk, G. Brenner-Weiss, R. R. Schmidt, and K. Sandhoff. 1990. Modulation of sphingolipid biosynthesis in primary cultured neurons by long chain bases. *J. Biol. Chem.* **265:** 9333–9339.
3. Merrill, A. H., and D. D. Jones. 1990. An update of the enzymology and regulation of sphingomyelin metabolism. *Biochim. Biophys. Acta.* **1044:** 1–12.
4. Huitema, K., J. van den Dikkenber, J. F. Brouwers, and J. C. Holthuis. 2004. Identification of a family of animal sphingomyelin synthases. *EMBO J.* **23:** 33–44.
5. Slotte, J. P. 2013. Biological functions of sphingomyelins. *Prog. Lipid Res.* **52:** 424–437.
6. Tafesse, F. G., K. Huitema, M. Hermansson, S. van der Poel, J. van den Dikkenberg, A. Uphoff, P. Somerharju, and J. C. M. Holthuis. 2007. Both sphingomyelin synthases SMS1 and SMS2 are required for sphingomyelin homeostasis and growth in human HeLa cells. *J. Biol. Chem.* **282:** 17537–17547.

JOURNAL OF LIPID RESEARCH ASBMB

7. Li, Z., T. K. Hailemariam, H. Zhou, Y. Li, D. C. Duckworth, D. A. Peake, Y. Zhang, M. S. Kuo, G. Cao, and X. C. Jiang. 2007. Inhibition of sphingomyelin synthase (SMS) affects intracellular sphingomyelin accumulation and plasma membrane lipid organization. *Biochim. Biophys. Acta.* **1771:** 1186–1194.
8. Subathra, M., A. Qureshi, and C. Luberto. 2011. Sphingomyelin synthases regulate protein trafficking and secretion. *PLoS ONE.* **6:** e23644.
9. Simons, K., and E. Ikonen. 1997. Functional rafts in cell membranes. *Nature.* **387:** 569–572.
10. Simons, K., and G. van Meer. 1988. Lipid sorting in epithelial cells. *Biochemistry.* **27:** 6197–6202.
11. Brown, D. A., and J. K. Rose. 1992. Sorting of GPI-anchored proteins to glycolipid-enriched membrane subdomains during transport to the apical cell surface. *Cell.* **68:** 533–544.
12. Parton, R. G., and K. Simons. 1995. Digging into caveolae. *Science.* **269:** 1398–1399.
13. Laux, T., K. Fukami, M. Thelen, T. Golub, D. Frey, and P. Caroni. 2000. Gap43, Marcks, and Cap23 modulate Pi(4,5)p2 at plasmalemmal rafts, and regulate cell cortex actin dynamics through a common mechanism. *J. Cell Biol.* **149:** 1455–1472.
14. Caroni, P. 2001. New EMBO members' review: actin cytoskeleton regulation through modulation of PI(4,5)P(2) rafts. *EMBO J.* **20:** 4332–4336.
15. Giepmans, B. N., and S. C. van Ijzendoorn. 2009. Epithelial cell-cell junctions and plasma membrane domains. *Biochim. Biophys. Acta.* **1788:** 820–831.
16. Adams, C. L., W. J. Nelson, and S. J. Smith. 1996. Quantitative analysis of cadherin-catenin-actin reorganization during development of cell-cell adhesion. *J. Cell Biol.* **135:** 1899–1911.
17. Márquez, M. G., N. O. Favale, F. Leocata Nieto, L. G. Pescio, and N. Sterin-Speziale. 2012. Changes in membrane lipid composition cause alterations in epithelial cell-cell adhesion structures in renal papillary collecting duct cells. *Biochim. Biophys. Acta.* **1818:** 491–501.
18. Bacallao, R., C. Antony, C. Dotti, E. Karsenti, E. H. Stelzer, and K. Simons. 1989. The subcellular organization of Madin-Darby canine kidney cells during the formation of a polarized epithelium. *J. Cell Biol.* **109:** 2817–2832.
19. Cavey, M., M. Rauzi, P. F. Lenne, and T. Lecuit. 2008. A two-tiered mechanism for stabilization and immobilization of E-cadherin. *Nature.* **453:** 751–756.
20. Tsukita, S., A. Nagafuchi, and S. Yonemura. 1992. Molecular linkage between cadherins and actin filaments in cell-cell adherens junctions. *Curr. Opin. Cell Biol.* **4:** 834–839.
21. Leckband, D., and A. Prakasam. 2006. Mechanism and dynamics of cadherin adhesion. *Annu. Rev. Biomed. Eng.* **8:** 259–287.
22. Knust, E., and O. Bossinger. 2002. Composition and formation of intercellular junctions in epithelial cells. *Science.* **298:** 1955–1959.
23. Nelson, W. J. 2003. Epithelial cell polarity from the outside looking in. *Physiology (Bethesda).* **18:** 143–146.
24. Guillot, C., and T. Lecuit. 2013. Mechanics of epithelial tissue homeostasis and morphogenesis. *Science.* **340:** 1185–1189.
25. Pescio, L. G., N. O. Favale, M. G. Marquez, and N. B. Sterin-Speziale. 2012. Glycosphingolipid synthesis is essential for MDCK cell differentiation. *Biochim. Biophys. Acta.* **1821:** 884–894.
26. Favale, N. O., N. B. Sterin Speziale, and M. C. Fernandez Tome. 2007. Hypertonic-induced lamin A/C synthesis and distribution to nucleoplasmic speckles is mediated by TonEBP/NFAT5 transcriptional activator. *Biochem. Biophys. Res. Commun.* **364:** 443–449.
27. Favale, N. O., M. C. Fernandez-Tome, L. G. Pescio, and N. B. Sterin-Speziale. 2010. The rate-limiting enzyme in phosphatidylcholine synthesis is associated with nuclear speckles under stress conditions. *Biochim. Biophys. Acta.* **1801:** 1184–1194.
28. Casali, C. I., K. Weber, N. O. Favale, and M. C. F. Tome. 2013. Environmental hyperosmolality regulates phospholipid biosynthesis in the renal epithelial cell line MDCK. *J. Lipid Res.* **54:** 677–691.
29. Fewster, M. E., B. J. Burns, and J. F. Mead. 1969. Quantitative densitometric thin-layer chromatography of lipids using copper acetate reagent. *J. Chromatogr. A.* **43:** 120–126.
30. Bartlett, G. R. 1959. Phosphorus assay in column chromatography. *J. Biol. Chem.* **234:** 466–468.
31. van Echten-Deckert, G. 2000. Sphingolipid extraction and analysis by thin-layer chromatography. *Methods Enzymol.* **312:** 64–79.
32. Oresti, G. M., P. L. Ayuza Aresti, G. Gigola, L. E. Reyes, and M. I. Aveldaño. 2010. Sequential depletion of rat testicular lipids with long-chain and very long-chain polyenoic fatty acids after X-ray-induced interruption of spermatogenesis. *J. Lipid Res.* **51:** 2600–2610.
33. Yamaji, A., Y. Sekizawa, K. Emoto, H. Sakuraba, K. Inoue, H. Kobayashi, and M. Umeda. 1998. Lysenin, a novel sphingomyelin-specific binding protein. *J. Biol. Chem.* **273:** 5300–5306.
34. Barceló-Coblijn, G., M. L. Martin, R. F. M. de Almeida, M. A. Noguera-Salvà, A. Marcilla-Etxenike, F. Guardiola-Serrano, A. Lüth, B. Kleuser, J. E. Halver, and P. V. Escribá. 2011. Sphingomyelin and sphingomyelin synthase (SMS) in the malignant transformation of glioma cells and in 2-hydroxyoleic acid therapy. *Proc. Natl. Acad. Sci. USA.* **108:** 19569–19574.
35. van Helvoort, A., W. van't Hof, T. Ritsema, A. Sandra, and G. van Meer. 1994. Conversion of diacylglycerol to phosphatidylcholine on the basolateral surface of epithelial (Madin-Darby canine kidney) cells. Evidence for the reverse action of a sphingomyelin synthase. *J. Biol. Chem.* **269:** 1763–1769.
36. Ternes, P., J. F. H. M. Brouwers, J. van den Dikkenberg, and J. C. M. Holthuis. 2009. Sphingomyelin synthase SMS2 displays dual activity as ceramide phosphoethanolamine synthase. *J. Lipid Res.* **50:** 2270–2277.
37. Ishitsuka, R., A. Yamaji-Hasegawa, A. Makino, Y. Hirabayashi, and T. Kobayashi. 2004. A lipid-specific toxin reveals heterogeneity of sphingomyelin-containing membranes. *Biophys. J.* **86:** 296–307.
38. Gumbiner, B. M. 1996. Cell adhesion: the molecular basis of tissue architecture and morphogenesis. *Cell.* **84:** 345–357.
39. Vasioukhin, V., C. Bauer, M. Yin, and E. Fuchs. 2000. Directed actin polymerization is the driving force for epithelial cell-cell adhesion. *Cell.* **100:** 209–219.
40. Vasioukhin, V., and E. Fuchs. 2001. Actin dynamics and cell–cell adhesion in epithelia. *Curr. Opin. Cell Biol.* **13:** 76–84.
41. Palovuori, R., R. Sormunen, and S. Eskelinen. 2003. SRC-induced disintegration of adherens junctions of Madin-Darby canine kidney cells is dependent on endocytosis of cadherin and antagonized by Tiam-1. *Lab. Invest.* **83:** 1901–1915.
42. Cavey, M., and T. Lecuit. 2009. Molecular bases of cell–cell junctions stability and dynamics. *Cold Spring Harb. Perspect. Biol.* **1:** a002998.
43. Yap, A. S., W. M. Brieher, and B. M. Gumbiner. 1997. Molecular and functional analysis of cadherin-based adherens junctions. *Annu. Rev. Cell Dev. Biol.* **13:** 119–146.
44. Baum, B., and M. Georgiou. 2011. Dynamics of adherens junctions in epithelial establishment, maintenance, and remodeling. *J. Cell Biol.* **192:** 907–917.
45. Desclozeaux, M., J. Venturato, F. G. Wylie, J. G. Kay, S. R. Joseph, H. T. Le, and J. L. Stow. 2008. Active Rab11 and functional recycling endosome are required for E-cadherin trafficking and lumen formation during epithelial morphogenesis. *Am. J. Physiol. Cell Physiol.* **295:** C545–C556.
46. Thompson, A., R. Nessler, D. Wisco, E. Anderson, B. Winckler, and D. Sheff. 2007. Recycling endosomes of polarized epithelial cells actively sort apical and basolateral cargos into separate subdomains. *Mol. Biol. Cell.* **18:** 2687–2697.
47. Lock, J. G., and J. L. Stow. 2005. Rab11 in recycling endosomes regulates the sorting and basolateral transport of E-cadherin. *Mol. Biol. Cell.* **16:** 1744–1755.
48. Gagescu, R., N. Demaurex, R. G. Parton, W. Hunziker, L. A. Huber, and J. Gruenberg. 2000. The recycling endosome of Madin-Darby canine kidney cells is a mildly acidic compartment rich in raft components. *Mol. Biol. Cell.* **11:** 2775–2791.
49. Yachi, R., Y. Uchida, B. H. Balakrishna, G. Anderluh, T. Kobayashi, T. Taguchi, and H. Arai. 2012. Subcellular localization of sphingomyelin revealed by two toxin-based probes in mammalian cells. *Genes Cells.* **17:** 720–727.